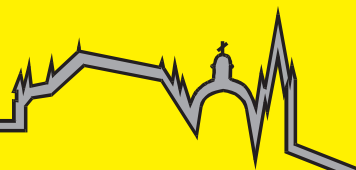


Marek Sebastian Simon

On the Mechanism of Evaporation-Determined Arc-Cathode Coupling in GMA Welding

Aachener Berichte Fügetechnik
Herausgeber: Prof. Dr.-Ing. U. Reisgen



Band 1/2021

Shaker Verlag

“On the Mechanism of Evaporation-Determined Arc-Cathode Coupling in GMA Welding”

„Über den Wirkzusammenhang der Verdampfungsbestimmten Kopplung von Lichtbogen und Kathode beim MSG-Schweißen“

Von der Fakultät für Maschinenwesen der Rheinisch-Westfälischen Technischen Hochschule Aachen zur Erlangung des akademischen Grades eines Doktors der Naturwissenschaften genehmigte Dissertation

vorgelegt von
Marek Sebastian Simon

Berichter: Univ.-Prof. Dr.-Ing. Uwe Reisgen
Univ.-Prof. Dr.rer.nat. Dirk Uhrlandt

Tag der mündlichen Prüfung: 22.04.2021

Diese Dissertation ist auf den Internetseiten der Universitätsbibliothek online verfügbar.

Marek Sebastian Simon

On the Mechanism of Evaporation-Determined Arc-Cathode Coupling in GMA Welding

Aachener Berichte Fügetechnik
Herausgeber: Prof. Dr.-Ing. U. Reisgen

Band 1/2021

Shaker Verlag

Bibliographic information published by the Deutsche Nationalbibliothek

The Deutsche Nationalbibliothek lists this publication in the Deutsche Nationalbibliografie; detailed bibliographic data are available in the Internet at <http://dnb.d-nb.de>.

Zugl.: D 82 (Diss. RWTH Aachen University, 2021)

Copyright Shaker Verlag 2021

All rights reserved. No part of this publication may be reproduced, stored in a retrieval system, or transmitted, in any form or by any means, electronic, mechanical, photocopying, recording or otherwise, without the prior permission of the publishers.

Printed in Germany.

ISBN 978-3-8440-8030-8

ISSN 0943-9358

Shaker Verlag GmbH • Am Langen Graben 15a • 52353 Düren

Phone: 0049/2421/99011-0 • Telefax: 0049/2421/99011-9

Internet: www.shaker.de • e-mail: info@shaker.de

Danksagung

Die vorliegende Arbeit entstand während meiner Tätigkeit als wissenschaftlicher Mitarbeiter am Institut für Schweißtechnik und Fügetechnik der Rheinisch-Westfälischen Technischen Hochschule Aachen mit finanzieller Unterstützung der Deutschen Forschungsgemeinschaft im Rahmen des SFB1120 „Präzision aus Schmelze“.

Zunächst möchte ich Gott danken, da ich durch die Kirche die Werte der Hingabe und der Ordnung gelernt habe, ohne die ich diese Arbeit nicht bewältigen hätte können.

Als nächstes gilt mein besonderer Dank dem Institutsleiter, Herrn Prof. Dr.-Ing. Uwe Reisgen, für seine Bereitschaft, mir die Möglichkeit zur Promotion gegeben zu haben, für die Betreuung meiner Arbeit, für das Vertrauen, das er in mich gesetzt hat und für die Ermutigung, die ich durch ihn erfahren habe. Herrn Prof. Dr.rer.nat. Dirk Uhrlandt danke ich für die sorgfältige Durchsicht der Arbeit, die Übernahme des Koreferates sowie seine ermutigende Beurteilung meiner Arbeit. Außerdem möchte ich auch Herrn Prof. Marek Behr (Ph.D.) für die Übernahme des Vorsitzes der Promotionskommission danken.

Als nächstes danke ich meinem Gruppenleiter Dr.-Ing. Oleg Mokrov sowie meinen beiden Oberingenieuren Dr.-Ing. Alexander Schiebahn und Herrn Rahul Sharma für ihr Vertrauen, sowie für ihre umsichtige Leitung meiner Arbeit und die vielen unschätzbar wertvollen Diskussionen, von denen ich maßgeblich profitiert habe.

Mein außerordentlicher Dank gilt Prof. Mikhail Benilov von der Universität von Madeira, für seinen Willen mich zu unterstützen und für seine Einladung zu einem Forschungsaufenthalt an die Universidade da Madeira.

Außerdem möchte ich mich bedanken bei meinen Kollegen vom SFB 1120 für die fruchtbare Arbeit in den Arbeitskreisen, sowie bei meinen Kollegen am ISF, insbesondere Dr.-Ing. Oleksii Lisnyi, Herrn Andre Schmidt, Herrn Philipp Lozano, Herrn Sobhan Emadmostoufi, Frau Gertrud Baumann sowie Dr.-Ing. Lars Stein, für ihre tatkräftige Unterstützung und Hilfsbereitschaft.

Zu guter Letzt gilt mein Dank meinen Freunden und meiner Familie, insbesondere meinen Eltern, Beata und Stefan Simon, sowie meiner Freundin Nazira Ibrahim für die Unterstützung und Liebe, die ich immer von ihnen erfahren habe.

Aachen im April 2021

Acknowledgements

This thesis was written during my work as scientific assistant at the Welding and Joining Institute at RWTH Aachen University with financial support of the German Research Foundation within the framework of the SFB1120 "Precision melt engineering".

First of all, I would like to thank God, because through the church I have learned the values of devotion and order, without which I would not have been able to accomplish this work.

My special thanks go to the head of the institute, Prof. Dr.-Ing. Uwe Reisgen, for his willingness to give me the opportunity to obtain a doctorate, and supervising of my work, for the trust he placed in me and his encouragement. I would like to thank Prof. Dr.rer.nat. Dirk Uhrlandt for the careful review of my work, for acting as assessor and for his encouraging evaluation. I would also like to thank Prof. Marek Behr (Ph.D.) for assuming the chairmanship of the doctoral committee.

Next, I would like to thank my group leader Dr.-Ing. Oleg Mokrov as well as my two head engineers Dr.-Ing. Alexander Schiebahn and Mr. Rahul Sharma for their trust, as well as for their prudent guidance of my work and many invaluable discussions from which I benefited significantly.

My sincere thanks go to Prof. Mikhail Benilov of the Universidade da Madeira for his willingness to support me in my research and his invitation to a research stay at the University of Madeira.

I would also like to thank my colleagues from SFB 1120 for the fruitful work in the working groups, as well as my colleagues at ISF, especially Dr.-Ing. Oleksii Lisnyi, Mr. Andre Schmidt, Mr. Philipp Lozano, Mr. Sobhan Emadmostoufi, Ms. Gertrud Baumann and Dr.-Ing. Lars Stein, for their active support and helpfulness.

Last but not least I would like to thank my friends and my family, especially my parents, Beata and Stefan Simon, as well as my girlfriend Nazira Ibrahim for the continuous support and overflowing love I have always received from them.

Aachen, April 2021

Excerpts from this work have already appeared in:

MOKROV, O., O. LYSNYI, M. SIMON, U. REISGEN, G. LASCHET, and M. APEL, 2017. Numerical investigation of droplet impact on the welding pool in gas metal arc welding [online]. *Materialwissenschaft und Werkstofftechnik*, **48**(12), 1206-1212. Available from: doi:10.1002/mawe.201700147

MOKROV, O., M. SIMON, R. SHARMA, and U. REISGEN, 2019. Arc-cathode attachment in GMA welding [online]. *Journal of Physics D: Applied Physics*, **52**(36), 364003. Available from: doi:10.1088/1361-6463/ab2bd9

MOKROV, O., M. SIMON, A. SCHIEBAHN und U. REISGEN, 2020. Concept for the calculation of the distribution of heat input in the cathode area by GMA welding [online]. *Welding in the World*, **34**(3), R103. Available from: doi:10.1007/s40194-020-00929-9

MOKROV, O., M. SIMON, R. SHARMA und U. REISGEN, 2020. Effects of evaporation-determined model of arc-cathode coupling on weld pool formation in GMAW process simulation [online]. *Welding in the World*, **64**(5), 847-856. Available from: doi:10.1007/s40194-020-00878-3

MOKROV, O., M. SIMON, P. LOZANO, D. ARNTZ-SCHROEDER, R. SHARMA und U. REISGEN, 2020. Simulation des Lichtbogenansatzes beim MSG-Schweißen. *DVS-Berichte, Band 365 : DVS Congress. Große Schweißtechnische Tagung. DVS CAMPUS. Vorträge der Online-Veranstaltungen vom 14. bis 18. September 2020.* pp. 700 - 706

I Content

I	Content.....	I
II	List of figures	V
III	List of tables	X
IV	List of abbreviations.....	XI
V	List of symbols.....	XIV
VI	Abstract	XXII
1	Introduction.....	1
1.1	Gas metal arc welding	1
1.2	The arc in GMAW.....	2
1.2.1	Plasma column.....	3
1.2.2	Plasma-electrode boundary layers	4
1.2.2.1	Anode layer	4
1.2.2.2	Cathode layer	5
2	State of the art.....	8
2.1	Substitution models used in GMAW process simulation	8
2.2	Cathode layer models derived from plasma physics	10
2.2.1	Models for arc-cathode coupling in diffuse arc attachment with a “hot cathode” at atmospheric pressure in inert gas:.....	10
2.2.1.1	PhD thesis of Kaddani. 1995	11
2.2.1.2	PhD thesis of Wendelstorf. 2000	12
2.2.1.3	PhD thesis by Cayla. 2008	14
2.2.1.4	PhD thesis by Shirvan. 2016	14
2.2.1.5	Benilov Marotta (1995) – „A model of the cathode region of atmospheric pressure arcs”	15
2.2.2	Models for cold cathodes	19

2.2.2.1 PhD thesis Coulombe (1997): Model for evaporating Cu, Fe, Ti cathodes	19
2.2.2.2 Models by Benilov (2015) and Almeida (2013) for vacuum arcs on evaporating Cr or CrCu cathodes.	24
2.2.2.3 Model of Benilov (1993) for “spot attachment” in vacuum arc for copper cathodes	28
2.3 Discussion	30
3 Statement of the problem and goals.....	33
3.1 Preliminary welding experiments (high speed video recordings).....	33
3.1.1 Welding experiments with helium.....	34
3.1.2 Welding experiments with Ar+8%CO ₂	37
3.2 Dialectic argument.....	40
3.2.1 Hypothesis 1: Ion flux due to evaporated atoms, ionized in the near-cathode plasma at constant temperature	42
3.2.1.1 Analysis	42
3.2.1.2 Conclusions	47
3.2.2 Hypothesis 2: Ion flux due to constant metal vapor density in the plasma	
48	
3.2.2.1 Analysis	48
3.2.2.2 Conclusions	53
3.2.3 Synthesis: proposal of core hypothesis.....	54
3.3 Conclusion	54
3.4 Goal of the work	55
3.4.1 Problem solving approach.....	55
4 Model description	56
4.1 Model for diffuse arc-cathode attachment	56
4.1.1 Theory of the model of the evaporation-determined arc cathode coupling (EDACC)	56

4.1.1.1 Heat fluxes.....	56
4.1.1.2 Electrical current densities.....	58
4.1.2 Results of the model for the evaporation-determined arc-cathode coupling	61
4.1.2.1 Composition of the heat flux and dominating mechanisms	61
4.1.2.2 Dependence of the heat flux and current density on $T_{\text{plasma,bulk}}$	67
4.1.2.3 Dependence of the heat flux and current density on UD	68
4.2 Discussion.....	70
5 Results: Coupling of the EDACC model to the weld pool	72
5.1 Set up for numerical CFD experiments	72
5.1.1 The domain	73
5.1.2 The material	74
5.1.3 The boundaries	76
5.1.3.1 Inlet.....	76
5.1.3.2 Outlet.....	76
5.1.3.3 Top	76
5.1.3.4 Bottom	76
5.1.3.5 Wall.....	76
5.1.3.6 Droplets	77
5.1.3.7 Arc heat and current	77
5.1.3.8 Evaporation	77
5.2 Sensitivity analysis	78
5.2.1 Analysis of the surface temperature field	80
5.2.2 Analysis of the heat flux and current density distributions	83
5.2.3 Analysis of the current density vector fields on the melting isosurface and the electromagnetic force in the weld pool	87
5.2.4 Analysis of the velocity vector fields in the weld pool.....	91

5.3 Discussion.....	94
6 Conclusions and Outlook.....	95
7 References	103
A Appendix: Model for evaporation by Knight (1979)	111

II List of figures

Abbildungsverzeichnis

Figure 1: Schematic of the Gas Metal Arc Welding process [MOK19].....	1
Figure 2: Example for stable voltage wire feed combinations in constant voltage GMA processes [REI15]	2
Figure 3: Calculated ratio of the flux of vaporized atoms to the flux of thermo-field emitted electrons as a function of the cathode surface temperature T_s for different cathode materials, from [COU97]	6
Figure 4: Schematic of the model for cathode region after Kaddani [KAD95].....	12
Figure 5: Schematic of the cathode layer as applied by Wendelstorf [WEN00].....	13
Figure 6: Resulting heat flux from [BEN95]. Full curves, broken curves and dotted curves take into account different ionization states of argon.	17
Figure 7: Densities of energy flux, ion current, electron emission, back-diffused electrons, electron temperature, ionization degree ω , the ratio of the energies delivered by the plasma electrons and by the ions rei and the ratio of cooling/heating rch , for $U = 17V$, from [BEN95].	18
Figure 8: Schematic representation of the cathode region of an emitting cathode exposed to a high pressure arc, from [COU97]	19
Figure 9: Ratio of ion current density to the current density due to thermo-field emission, from [COU97]	21
Figure 10: Ratio of flux of vaporization and flux by thermo-field emission for copper in dependence of electron temperature and saturated vapor pressure from the heated cathode surface, from [COU97]	22
Figure 11: Heat flux to a copper cathode in an atmospheric arc cathode spot, from [COU97].....	23
Figure 12: Current density to a copper cathode in an atmospheric arc cathode spot from [COU97]	24

Figure 13: Ion saturation current for Cr-vapor plasma, $Te = 8000[K]$, $ji(d)$: diffusion approach, $ji(f)$: multi-fluid approach; d : ionization length; λD : Debye-length; λia : mean free path for collisions between ions an neutrals, from [BEN15].....	25
Figure 14: Schematic of the double sheath approach with ionisation of emitted atoms, from [BEN10]	26
Figure 15: Electric current density j for Cu (solid) and Cr (dashed), for different cathode layer voltages, from [ALM13].....	27
Figure 16: Heat flux from the plasma to the cathode q for Cu (solid) and Cr (dashed) cathode with different cathode layer voltages from [ALM13]	28
Figure 17: Heat flux as resulting for a copper cathode in a vacuum arc, in dependence of cathode layer voltage drop and inverse cathode surface temperature $Tw - 1$, from [BEN93]	29
Figure 18: Transient Current-Voltage recordings for helium shielding gas, with $vweld = 60[cmm\text{in}]$. U_{total} , $average = 36[V]$, $I = 193[A]$	34
Figure 19: Identifiable cathode spots (marked with red circles on the right side) in helium, with $vweld = 60[cmm\text{in}]$. Aperture 22; UV+ND4 Filter. No spectral filter. 30000fps. $1/30000[s]$ shutter time. [MOK20b]	35
Figure 20: a) calm and smooth weld pool surface in the case with spot attachment, see Figure 19. b) rough weld pool surface at weld pool attachment. Shielding gas: helium, with $vweld = 60[cmm\text{in}]$. The arc is burning directly on the melt pool. Aperture 22; UV+ND4 Filter. 436nm spectral filter. 30000fps. $1/1000000[s]$ shutter time. [MOK20b]	36
Figure 21: Appearance of dry islands (marked in red on the right side) in helium with $vweld = 90[cmm\text{in}]$, in the phase with "spot attachment". Aperture 22, UV+ND4 Filter. 436nm spectral filter. 30000fps. $1/1000000[s]$ shutter time.	37
Figure 22: Transient Current-Voltage recordings for argon+8%CO ₂ shielding gas, with $vweld = 60[cmm\text{in}]$. U_{total} , $average = 28[V]$, I_{total} , $average = 197[A]$	38
Figure 23: Three consecutive moments of the weld pool in Ar+8%CO ₂ at $vweld = 60[cmm\text{in}]$. No spots are identifiable, but only an extending "white zone" ahead of the melting front. Aperture 22, UV+ND2 Filter. No spectral filter. 30000fps. $1/1000000[s]$ shutter time. [MOK20b].....	39

Figure 24: Three consecutive close-ups of the "white zone" in Ar+8%CO ₂ at $v_{weld} = 60[\text{cmmin}]$. Spots are not identifiable. Aperture 22, UV+ND2 Filter. No spectral filter. 225000fps.	1/225000[s] shutter time. [MOK20b]	39
Figure 25: Current density due to field enhanced thermionic emission, with fixed ion current density j_{ion} for the Mackeown formula		41
Figure 26: Heat fluxes according to the assumption of full ionization of the evaporated atoms and their return to the cathode		42
Figure 27: Current density according to the assumption of full ionization of the evaporated atoms and their return to the cathode		43
Figure 28: Ionization degree for the assumption that evaporated iron atoms are ionized at $T_{plasma} = 7000[K]$		44
Figure 29: Heat flux to the cathode, assuming ionization of evaporated iron atoms in LTE at $T_{plasma} = 7000[K]$		45
Figure 30: Current density to the cathode, assuming ionization of evaporated iron atoms in LTE at $T_{plasma} = 7000[K]$		46
Figure 31: Hypothetical surface temperature of a weld pool calculation assuming ionization of evaporated atoms at $T_{plasma} = 6500[K]$. The current as well as the evaporation losses are unrealistically high.		47
Figure 32: Heat flux to the cathode, assuming ionization of a constant density of iron atoms in LTE at $T_{plasma} = 7000[K]$		49
Figure 33: Current density to the cathode, assuming ionization of a constant density of iron atoms in LTE at $T_{plasma} = 7000[K]$		50
Figure 34: Hypothetical surface temperature of a weld pool calculation assuming ionization of a constant density of iron atoms in LTE at $T_{plasma} = 7000[K]$. Losses due to evaporation are significant		51
Figure 35: Saturated vapor density $n_{vap}(ps)$ compared with the constant iron atom density $n_{Fe} = \text{const.}$		52
Figure 36: Comparison of ionized atoms at LTE with constant $T_{plasma} = 7000[K]$, once due to constant density and once due to saturated vapor pressure		53

Figure 37: The ion density in LTE for <i>T_{plasma, local}</i> modified by metal vapor according to Eq.(14), assuming <i>T_{plasma, bulk} = 7000[K]</i> , showing the behavior when considering only ionization of atoms from vapor or from the plasma bulk, and their combined influence.....	60
Figure 38: Heat flux according to the model presented in 4.1.1, with <i>UD = 17[V]</i> and <i>T_{plasma, bulk} = 7000[K]</i>	62
Figure 39: Heat flux according to the model presented in 4.1.1, with <i>UD = 17[V]</i> and <i>T_{plasma, bulk} = 12000[K]</i>	64
Figure 40: Comparison of current density due to ions and due to field-enhanced thermionic emission.....	65
Figure 41: Ionization degree according to the model presented in 4.1.1, with <i>T_{plasma, bulk} = 7000[K]</i>	66
Figure 42: <i>T_{plasma, local}</i> for different <i>T_{plasma, bulk}</i>	66
Figure 43: Heat flux dependency on <i>T_{plasma, bulk}</i> , with indication of the cathode surface temperature with maximum heat flux	67
Figure 44: Current density dependency on <i>T_{plasma, bulk}</i> , with indication of the cathode surface temperature with maximum current density.....	68
Figure 45: Heat flux dependency on <i>UD</i> , with fixed temperature of the plasma bulk <i>T_{plasma, bulk} = 7000[K]</i>	69
Figure 46: Current density dependency on <i>UD</i> , with fixed temperature of the plasma bulk <i>T_{plasma, bulk} = 7000[K]</i>	70
Figure 47: Computational domain for the weld pool calculation including mesh.....	74
Figure 48: Specific Heat, thermal conductivity and electrical conductivity, as used, from [MOK17] (temperature ranges were extrapolated)	75
Figure 49: Heat flux due to evaporation, according to Knight model [KNI79]	78
Figure 50: Surface temperature field with weld pool depth, width and length indicated, as well as maximum temperature. The black contour line gives the melting isothermal. a) was published in [MOK20b].....	80
Figure 51: Cross Sections with weld pool depth, width and length indicated, as well as maximum temperature.....	81

Figure 52: Comparison between Gaussian (a) and EDACC (b) heat flux distribution for basic case.....	83
Figure 53: Heat flux distribution due to the EDACC model, with total current, total net heating power as well as total heat losses by evaporation indicated, as well as the maximum heat flux indicated. a) was published in [MOK20b].....	84
Figure 54: Current density distribution due to the EDACC model, with total current indicated. a) was published in [MOK20b]	85
Figure 55: Current density vector field on the melting iso-surface, with the maximum current density indicated. Welding direction from left to right.....	89
Figure 56: Electromagnetic force density in the melt pool, with the maximum value indicated. Welding direction from left to right	90
Figure 57: Flow velocity in the melt pool, with the maximum value indicated. Welding direction from left to right.	92
Figure 58: Flow velocity streamlines in the weld pool, with the maximum velocity indicated	93
Figure 59: Subsonic flow structure, from [KNI79]	111

III List of tables*Tabellenverzeichnis*

Table 1: Reference index for the overview of results.....	79
---	----

IV List of abbreviations

Abkürzungsverzeichnis

	one dimensional
1D	<i>eindimensional</i>
	two dimensional
2D	<i>zweidimensional</i>
	three dimensional
3D	<i>dreidimensional</i>
AC-TIG	alternate current tungsten inertgas welding <i>Wechselstrom Wolfram-Inertgas-Schweißen</i>
Ansys CFX	commercial computational fluid dynamics software <i>kommerzielle Flüssigodynamik Software</i>
Ar	argon <i>Argon</i>
Ar+++	triple ionized argon <i>dreifach ionisiertes Argon</i>
CFD	computational fluid dynamics <i>rechnergestützte Strömungsdynamik</i>
CMT	“cold metal transfer” - mode of welding operation <i>“cold metal transfer” – eine Schweißtechnik</i>
CO ₂	carbon dioxide <i>Kohlenstoffdioxid</i>
Cr	chromium <i>Chrom</i>
Cu	copper <i>Kupfer</i>

	explosive centre electron emission mechanism
ECTON	<i>Elektronenemissionsmechanismus, der von Mikroexplosionen ausgeht</i>
EDACC	Evaporation Determined Arc-Cathode Coupling <i>Verdampfungsbestimmte Kopplung von Lichtbogen und Kathode</i>
Eq.	Equation <i>Gleichung</i>
ESAB	welding equipment manufacturer <i>Schweißzusatzwerkstoffhersteller</i>
EWM	welding equipment manufacturer <i>Schweißgerätehersteller</i>
Fe	iron <i>Eisen</i>
G3Si1	a welding wire quality <i>eine Schweißdrahtgüte</i>
GMAW/GMA	gas metal arc welding <i>Metallschutzgas Schweißen</i>
He	helium <i>Helium</i>
HTC	heat transfer coefficient <i>Wärmeübergangskoeffizient</i>
LTE	local thermodynamic equilibrium <i>lokales thermodynamisches Gleichgewicht</i>
MHD	magneto-hydrodynamic <i>Magnetohydrodynamik</i>
MSG	Metall-Schutzgas (=GMAW)

ND	neutral density filters <i>Neutraldichtefilter</i>
NEC	net emission coefficient <i>Nettoemissionskoeffizient</i>
O2	molecular oxygen <i>molekularer Sauerstoff</i>
OpenFOAM	an open source CFD software package <i>ein quelloffenes Softwarepaket für Strömungsdynamik</i>
PhD	academic degree of Doctor of Philosophy <i>akademischer Doktorgrad</i>
pLTE	partial thermodynamic equilibrium <i>teilweises thermodynamisches Gleichgewicht</i>
Ti	titanium <i>Titan</i>
TIG	tungsten inert gas <i>Wolfram Inertgas Schweißen</i>
UV	ultra violet <i>ultraviolett</i>
V	Volt <i>Volt</i>
W	tungsten <i>Wolfram</i>
WTWD	work piece to wire distance <i>Abstand zwischen Elektrodenspitze und Werkstück</i>
Zr	zirconium <i>Zirkonium</i>

V List of symbols

Formelzeichen

\vec{A}	$\left[\frac{N}{A} \right]$	Magnetic vector potential from [MOK17]
ΔA	$[eV]$	Lowering of the work function
A	$[eV]$	Work function ($4.5[eV]$ for iron)
A_{eff}	$[eV]$	Effective work function (work function with Schottky correction)
\vec{B}	$\left[\frac{N \cdot s}{C \cdot m} \right]$	Magnetic field vector from [MOK17]
β_A	$[K^{-1}]$	Thermal expansivity coefficient from [MOK17]
c_{ion}	$\left[\frac{m}{s} \right]$	Ion speed of sound
d	$[m]$	Thickness of the welded plate in the CFD simulations
d	$[m]$	Ionization length in [BEN15]
d_{wire}	$[m]$	Diameter of the wire
e	$[C]$	Elementary charge
ϵ_0	$\left[\frac{A \cdot s}{V \cdot m} \right]$	Vacuum permittivity
E_f	$\left[\frac{V}{m} \right]$	Electric field at the cathode surface
E_{ion}	$[eV]$	Ionization energy
E_{ion}	$[eV]$	First ionization energy
\vec{g}	$\left[\frac{m}{s^2} \right]$	Gravitational acceleration from [MOK17]
γ	$[-]$	Ratio of specific heats
Γ_{vap}	$\left[\frac{1}{m^2 s} \right]$	Rate of vaporization as used in [COU97]

h	[$J \cdot s$]	Planck constant
h	[J]	Enthalpy from [MOK17]
H	[$\frac{J}{mol}$]	Heat of vaporization
H_{vap}	[$\frac{J}{mol}$]	Condensation enthalpy
I	[A]	Total current
j	[$\frac{A}{m^2}$]	Current density
\vec{j}	[$\frac{A}{m^2}$]	Current density vector in [MOK17]
$j_{diffuse}$	[$\frac{A}{m^2}$]	Estimated current density for diffuse arc attachment
j_e	[$\frac{A}{m^2}$]	Current density due to back-diffused electrons in [BEN95]
j_{em}	[$\frac{A}{m^2}$]	Current density of field-enhanced thermionic or thermo-field emission
j_{em}	[$\frac{A}{m^2}$]	Current density due to field-enhanced thermionically emitted Electrons in [BEN95]
j_{em}	[$\frac{A}{m^2}$]	Current density due to thermo-field emission in [COU97]
$j_i^{(d)}$	[$\frac{A}{m^2}$]	Ion current density in diffusion approach in [BEN15]
$j_i^{(f)}$	[$\frac{A}{m^2}$]	Ion current density in multi-fluid approach in [BEN15]
j_i	[$\frac{A}{m^2}$]	Current density due to ion flux in [BEN95]
j_{ion}	[$\frac{A}{m^2}$]	Current density due to ions in [COU97]

j_{ion}	$\left[\frac{A}{m^2} \right]$	Current density due to ions
j_{spot}	$\left[\frac{A}{m^2} \right]$	Current density in the cathode spot
$j_{tot}(p_{max})$	$\left[\frac{A}{m^2} \right]$	Total current density at maximal vaporization pressure in [COU97]
j_{total}	$\left[\frac{A}{m^2} \right]$	Total current density
J_{em}	$\left[\frac{1}{m^2} \right]$	Particle flux of thermionically emitted electrons in [BEN95]
J_i	$\left[\frac{1}{m^2} \right]$	Ion particle flux in [BEN95]
J_{vap}	$\left[\frac{1}{m^2 s} \right]$	Flux of evaporated atoms in [BEN93]
J_{vap}	$\left[\frac{kg}{m^2 s} \right]$	Evaporated mass flux
k_B	$\left[\frac{J}{K} \right]$	Boltzmann constant
$k_{ionization}$	$\left[\frac{m^6}{s} \right]$	Ionization rate as used in [BEN95]
$k_{recombination}$	$\left[\frac{m^6}{s} \right]$	Recombination rate as used in [BEN95]
l_{Debye}	[m]	Debye length
l_{ion}	[m]	Length scale of ionization collisions
l_{therm}	[m]	Length scale of electron energy relaxation
λ	$\left[\frac{W}{m \cdot K} \right]$	Thermal conductivity from [MOK17]
λ_D	[m]	Debye-length in [BEN15]
λ_{ia}	[m]	Mean free path for collisions between ions and neutrals in [BEN15]
λ_u	[m]	Length of electron energy relaxation

λ_{vap}	[m]	Length of thermal influence of the metal vapor
μ_0	$\left[\frac{kg \cdot m}{s^2 \cdot A^2} \right]$	Magnetic vacuum permeability, also in [MOK17]
M_{Fe}	$\left[\frac{kg}{mol} \right]$	Molar mass of iron
\dot{m}	$\left[\frac{kg}{s} \right]$	Mass rate
m_{Fe}	[kg]	Atomic mass of iron
m_e	[kg]	Electron mass
m_{ion}	[kg]	Ion mass
n_0	$\left[\frac{1}{m^3} \right]$	Metal vapor particle density in the plasma bulk
n_{Ar}	$\left[\frac{1}{m^3} \right]$	Argon particle density
n_{Fe}	$\left[\frac{1}{m^3} \right]$	Iron vapor particle density
n_e	$\left[\frac{1}{m^3} \right]$	Electron particle density
n_i	$\left[\frac{1}{m^3} \right]$	Particle density of ions in [BEN15]
n_{ion}	$\left[\frac{1}{m^3} \right]$	Ion particle density
n_{ions}	$\left[\frac{1}{m^3} \right]$	Ion particle density
$n_{plasma,bulk}$	$\left[\frac{1}{m^3} \right]$	Particle density in the plasma bulk
n_{vap}	$\left[\frac{1}{m^3} \right]$	Density due to the saturated vapor pressure
N_A	$\left[\frac{1}{mol} \right]$	Avogadro constant

N_L	$\frac{1}{m^3}$	Loschmidt number
ν	[Pa s]	Viscosity
ω	[–]	Ionization degree in [BEN95]
p	[Pa]	Pressure, also in [MOK17]
p_{amb}	[Pa]	Ambient pressure
p_{atm}	[Pa]	Atmospheric pressure
p_{vap}	[Pa]	Saturated vapor pressure
P	[W]	Heat power
φ	[V]	Potential in [BEN15]
q	$\frac{W}{m^2}$	Heat flux
q_{cond}	$\frac{W}{m^2}$	Heat flux carried into the cathode
$q_{diffuse}$	$\left[\frac{W}{m^2}\right]$	Estimated heat flux for diffuse arc attachment
q_{em}	$\left[\frac{W}{m^2}\right]$	Heat flux due to electron emission
q_{evap}	$\left[\frac{W}{m^2}\right]$	Heat flux due to evaporation
q_{ion}	$\left[\frac{W}{m^2}\right]$	Heat flux due to ions
q_{max}	$\left[\frac{W}{m^2}\right]$	Maximum heat flux
q_{rad}	$\left[\frac{W}{m^2}\right]$	Heat flux due to radiation
q_{total}	$\left[\frac{W}{m^2}\right]$	Net heat flux
r_*	[m]	Radius of the cathode spot in [BEN95]
r_{HS}	[mm]	Radius of the heat source
r_{ch}	[–]	Ratio of cooling/heating in [BEN95]

$r_{droplet}$	[m]	Radius of the droplet
r_{ei}	[–]	Ratio of the energies delivered by the plasma electrons and by the ions in [BEN95]
R	$\left[\frac{kg \cdot m^2}{s^2 \cdot mol \cdot K} \right]$	Ideal gas constant
ρ	$\left[\frac{kg}{m^3} \right]$	Mass density from [MOK17]
ρ_{iron}	$\left[\frac{kg}{m^3} \right]$	Mass density of iron
ρ_k	$\left[\frac{kg}{m^3} \right]$	Mass density at the edge of the Knudsen layer
ρ_{wire}	$\left[\frac{kg}{m^3} \right]$	Mass density of the wire
$\overrightarrow{S}_{droplet,u}$	$\left[\frac{kg}{m^2 s^2} \right]$	Momentum source by droplets from [MOK17]
$S_{droplet,h}$	[W]	Enthalpy source by droplets from [MOK17]
σ	$\left[\frac{S}{m} \right]$	Electrical conductivity from [MOK17]
T	[K]	Temperature from [MOK17]
T_h	[K]	Heavy particle temperature
T_{amb}	[K]	Ambient temperature
$T_{boiling,copper}$	[K]	Boiling temperature of copper
$T_{boiling,iron}$	[K]	Boiling temperature of iron
$T_{droplet}$	[K]	Temperature of the droplet
T_e	[K]	Electron temperature
T_{e*}	[K]	Characteristic electron temperature in the near-cathode layer in [BEN95]
T_i	[K]	Ion temperature
T_{ion}	[K]	Ion temperature in [COU97]

T_k	[K]	Temperature at the edge of the Knudsen layer
T_{max}	[K]	Maximum temperature
T_{min}	[K]	Minimum temperature
$T_{plasma,bulk}$	[K]	Temperature of the plasma bulk
$T_{plasma,local}$	[K]	Local plasma temperature of the near-cathode plasma
T_{plasma}	[K]	Plasma temperature
T_{ref}, p_{ref}	[K], [Pa]	Temperature and pressure in reference state for CFD simulation
$T_{s,max}(q > 0)$	[K]	The maximum cathode surface temperature where the heat flux is still positive
T_s	[K]	Cathode surface temperature
$T_s(q_{max})$	[K]	The cathode surface temperature where the heat flux is at maximum
T_{vap}	[K]	Temperature of the vapor
$T_{w,max}(q > 0)$	[K]	The maximum cathode surface temperature where the heat flux is still positive
T_w	[K]	Cathode surface temperature as used in [BEN95] and [BEN15] and [ALM13]
$T_w(q_{max})$	[K]	The cathode surface temperature where the heat flux is at maximum
t	[s]	Time from [MOK17]
$t_{8/5}$	[s]	Measure for cooling time from 800°C to 500°C, as used in welding to determine formation of microstructure
v_{Bohm}	$\left[\frac{m}{s}\right]$	Bohm velocity
v_e	$\left[\frac{m}{s}\right]$	Electron velocity

v_{ion}	$\left[\frac{m}{s} \right]$	Ion velocity
v_{weld}	$\left[\frac{m}{min} \right]$	Welding velocity
v_{wire}	$\left[\frac{m}{min} \right]$	Wire feed velocity
x, y, z	$[m], [m], [m]$	Coordinates in the simulation domain
x_0	$[m]$	X-coordinate of center of the arc
y_0	$[m]$	Y-coordinate of center of the arc
\vec{u}	$\left[\frac{m}{s} \right]$	Flow velocity from [MOK17]
u_k	$\left[\frac{m}{s} \right]$	Bulk flow velocity at the edge of the Knudsen layer
U	$[V]$	Cathode layer voltage drop in [BEN95]
U_D	$[V]$	Cathode voltage drop
U_a	$[V]$	Anode voltage drop
V_c	$[V]$	Cathode voltage drop in [COU97]
Z_{Fe}	$[-]$	Partition function of iron atoms
Z_{Fe+}	$[-]$	Partition function of singly ionized iron ions
Z	$[-]$	Charge number of ions

VI Abstract

In gas metal arc welding (GMAW) process simulation, it is desired to predict the energy transferred to the process as well as the weld pool geometry. For this reason, the coupling of the arc to the welded material is of high interest, both at the cathode and anode. Although there exists a substantial body of work on the coupling of the arc to the cathode, the present models cannot be applied in the conditions of GMAW welding, as they give unphysical results. In particular, the current models usually result in very high cathode surface temperatures, i.e. above boiling temperature of the metals. After relevant experiments are presented and discussed, it is concluded that the current state of the art does not reflect the observations and that therefore a new approach needs to be developed. Furthermore, a dialectic argument is developed, namely that the coupling of the arc to the cathode in diffuse attachment of GMAW must be strongly determined by evaporation. The argument concludes that the current transfer is mainly carried by metal ions that are evaporated from the cathode surface and ionized in the near cathode plasma, and that this current transfer must be limited to below boiling temperature. The core hypothesis is that this limit results from a decrease of the ionization degree, due to cooling of the near cathode plasma by the cold metal vapor. Based on this argument, a mathematical model for the Evaporation-Determined Arc-Cathode Coupling (EDACC), is introduced in detail. The properties of the model are then analyzed by applying it to a simplified computational fluid dynamics (CFD) weld pool simulation and it shows that the model is in line with the observed cathode surface temperatures below boiling. Finally, also an outlook is given on possible applications of this new understanding of the arc-cathode coupling, as well as a discussion of open questions and current limitations of the model.

Kurzfassung

Bei der Prozesssimulation des Metall-Schutzgasschweißens ist es das Ziel, die auf den Prozess übertragene Energie sowie die Schweißbadgeometrie vorherzusagen. Aus diesem Grund ist die Kopplung des Lichtbogens an den geschweißten Werkstoff sowohl an der Kathode als auch an der Anode von herausragendem Interesse. Obwohl es einen umfangreichen Bestand an Arbeiten zur Kopplung des Lichtbogens an die Kathode gibt, können die vorliegenden Modelle unter den Bedingungen des MSG-Schweißens nicht angewendet werden, da sie unphysikalische Ergebnisse liefern. Insbesondere führen die aktuellen Modelle in der Regel zu sehr hohen Kathodenoberflächentemperaturen, d.h. oberhalb der Siedetemperatur der Metalle. Nachdem einschlägige Experimente vorgestellt und diskutiert wurden wird deutlich, dass der derzeitige Stand der Technik mit den Beobachtungen nicht in Einklang zu bringen ist und daher ein neuer Ansatz entwickelt werden muss. Weiterhin wird ein dialektisches Argument entwickelt, nämlich, dass die Kopplung des Lichtbogens an die Kathode unter den Bedingungen von diffuser Anbindung beim Metallschutzgassschweißen, als stark verdampfungsabhängig aufgefasst werden muss. Das Ergebnis dieser Argumentation ist die Schlussfolgerung, dass die Stromübertragung hauptsächlich von Metallionen getragen wird, die von der Kathodenoberfläche verdampft und im kathodennahen Plasma ionisiert werden, und dass diese Stromübertragung unterhalb des Siedepunkts begrenzt sein muss. Als Kernhypothese wird dann vorgeschlagen, dass diese Begrenzung durch eine Abnahme des Ionisationsgrades infolge der Abkühlung des kathodennahen Plasmas durch den kalten Metalldampf erfolgt. Auf dieser Argumentation aufbauend wird ein mathematisches Modell für die verdampfungsbestimmte Kopplung von Lichtbogen und Kathode (EDACC) eingehend vorgestellt. Die Eigenschaften des Modells werden dann in der Anwendung auf eine vereinfachte CFD-Schweißbadsimulation analysiert, und es zeigt sich, dass das Modell die beobachteten Kathodenoberflächentemperaturen unterhalb des Siedepunkts reproduziert. Schließlich werden noch ein Ausblick auf mögliche Anwendungen dieses neu gewonnenen Verständnisses über die Lichtbogen-Kathoden-Kopplung gegeben, sowie offene Fragen und gegenwärtige Begrenzungen des Modells diskutiert.

"Truth is much too complicated to allow anything but approximations"

- John von Neumann, 1947